Determining Thermal Properties of Polyurethane by Solving the Heat Equation and IR Imaging

H Eidesen[1], Z Andleeb[2], H Khawaja[1]*, M Moatamedi[3]

1. UiT-The Arctic University of Norway, Tromsø, Norway
2. Abyss Solutions, Islamabad, Pakistan
3. Al Ghurair University, Dubai, UAE

ABSTRACT

All materials have different and unique thermal properties that determine how the temperature changes when a material is subjected to a temperature difference. This study was intended to investigate the thermal properties of a polymer called Polyurethane, focusing on anti-seepage and anti-abrasion polyurethane. The thermal conductivity and heat transfer coefficient of cold polyurethane specimens have been calculated by capturing the infrared signature using a FLIR T1030Sc Infrared camera and comparing the results with simulated results. The simulations were carried out in MATLAB®, and the solution is based on the Heat equation. This paper describes the driving mechanisms behind the Heat equation and how the approximated solution to the Heat equation is obtained by discretizing through a forward-time central-space (FTCS) finite-difference method. The results reveal that the heat transfer coefficient for anti-abrasion Polyurethane is almost four times that for anti-seepage Polyurethane. The thermal conductivity for the respective has a difference of a factor of two. A good agreement between the experimental and the numerical study was achieved. This study is helpful for the potential use of polyurethane material in Arctic regions either as a coating material for pipes or as a sealant in the oil and gas industry.

1. INTRODUCTION

1.1. Fourier's law

Fourier's Law [1] can be applied to describe the heat transfer in spatial directions (x, y or z) per unit area perpendicular to the direction of transfer. Further, the heat transfer is proportional to the temperature gradient [2]. Fourier's Law, in $x - direction$ (one dimension), can be seen in Equation 1.

$$q = -k\frac{dT}{dx} \tag{1}$$

where the heat flux q is (Wm^{-2}), k is the thermal conductivity $Wm^{-1}K^{-1}$, x is spatial direction, dT/dx is the temperature gradient. Minus sign is added because energy is transferred from a higher temperature to a lower temperature medium.

---
*Corresponding Author: hassan.a.khawaja@uit.no

Two important constants determine the temperature of a body subjected to the heat change: the thermal conductivity k and the heat transfer coefficient h. The heat transfer coefficient describes the heat transfer rate to the body, whereas the thermal conductivity describes the rate the transferred heat dissipates within the body [3]. The symbols and units are k ($Wm^{-1}K^{-1}$) and h ($Wm^{-2}K^{-1}$), respectively.

The product of ρc, with units ($Jm^{-3}\ K^{-1}$), is often described as the material's ability to store heat (energy) and is called the volumetric heat capacity [2]. Further, to describe the rate at which the material reaches equilibrium temperature (e.g., adapt to ambient atmosphere), the thermal diffusivity constant, α with the units (m^3s^{-1}) can be stated in Equation 2:

$$\alpha = \frac{k}{\rho c} \tag{2}$$

Usually, materials with a large α will absorb heat at a faster rate compared to materials with a small α [2].

1.2. Heat Equation

The one-dimensional temperature field in a solid can be described as shown in Equation 3.

$$\frac{\partial T}{\partial t}\rho c = Q + \frac{\partial}{\partial x}\left(k\frac{\partial T}{\partial x}\right) \tag{3}$$

where ρ ($kg\ m^{-3}$) is density, c ($J\ kg^{-1}K^{-1}$) is heat capacity at constant pressure, Q (Wm^{-3}) is the volumetric energy generation term [4], T (K) is temperature field and t (s) is time. Equation (3) can be written in three spatial dimensions as shown in Equation (4).

$$\frac{\partial T}{\partial t} = \alpha(\frac{\partial^2 T}{\partial x^2} + \frac{\partial^2 T}{\partial y^2} + \frac{\partial^2 T}{\partial z^2}) \tag{4}$$

where x, y, and z refer to cartesian coordinates and volumetric energy generation term is neglected.

1.3. Infrared thermography

Infrared thermography is the science of detecting infrared energy emitted from an object. Literally, infrared thermography means "beyond red temperature image". IR thermography, being a remote non-contact/non-destructive means of testing, is perfectly suitable for tests in extreme environments [5]. In addition, it is fast, reliable, and detailed. Due to the advantages offered by IR thermography, it is extremely popular in various industries. Infrared thermography (IRT) has a long history in industrial applications. Moreover, its use is increasing exponentially in research and development sectors [6-10].

Cold climate operations face several challenges. Recent activity in the Arctic Circle has encouraged researchers to study the various challenges. Thermography is one such technique used for this purpose; it exploits the infrared wavelengths of the electromagnetic spectrum region from 0.75μm to 1mm [11]. Much like a visible light camera, an infrared camera uses a lens to focus the infrared light of different wavelengths emitted (thermal radiation) by all objects in view, which is converted into an electronic signal by infrared detectors. The signal is further processed digitally to create a thermal image. The basic setup of thermography is illustrated in Figure 1. The rate of energy emitted as thermal radiation is highly dependent on the surface temperature. Therefore, small temperature changes in the test specimens generate visible thermal readings that infrared detectors can successfully capture to yield thermogram [3, 12-14].
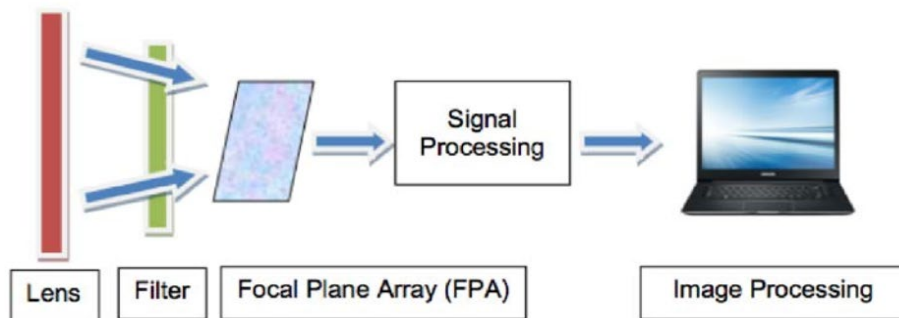

Figure 1: Basic setup of thermography testing

2. METHODOLOGY

2.1. Polyurethane Samples

Polyurethane was invented by Otto Bayer and Heinrich Rinke, in Germany in 1937 [15,16] and some of the first use of this plastic was during WWII, where it was applied as a coating on the German airplanes [17]. Polyurethane belongs to the chemical class called reaction polymers [18]. In this paper, the Polyurethane used is developed by China Institute of Water Resources & Hydropower Research Beijing IWHR-KHL Co. Ltd [19]. The product name is SK One Component Polyurethane; however, it will be referred as Polyurethane in this paper [20,21]. The company provided two distinct types of Polyurethane, namely anti-seepage Polyurethane and anti-abrasion polyurethane. Anti-seepage Polyurethane is suggested to be used as a sealant in either chemical tanks, as it has good resistance to chemical corrosion [22] or in dams to prevent water leaks through the concrete. Anti-abrasion Polyurethane can be used on locations where high corrosion is expected. Locations of such can be water ducts from dams, on ships, due to the force of water while ship is in transit, and so forth [23].

2.2. IR Imaging and Setup

The flow chart below in Figure 2 shows the basics steps elected to determine the heat transfer coefficient and thermal conductivity.
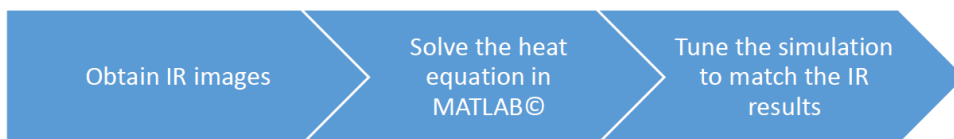

Figure 2: flow chart to determine heat transfer coefficient, h, and thermal conductivity, k.

The experiment used a FLIR T1030sc [24] camera to capture the infrared radiation of the polyurethane sample. The sample was oriented normal to the camera lens. The data was gathered inside the software. The schematic of the setup can be seen in Figure 3.
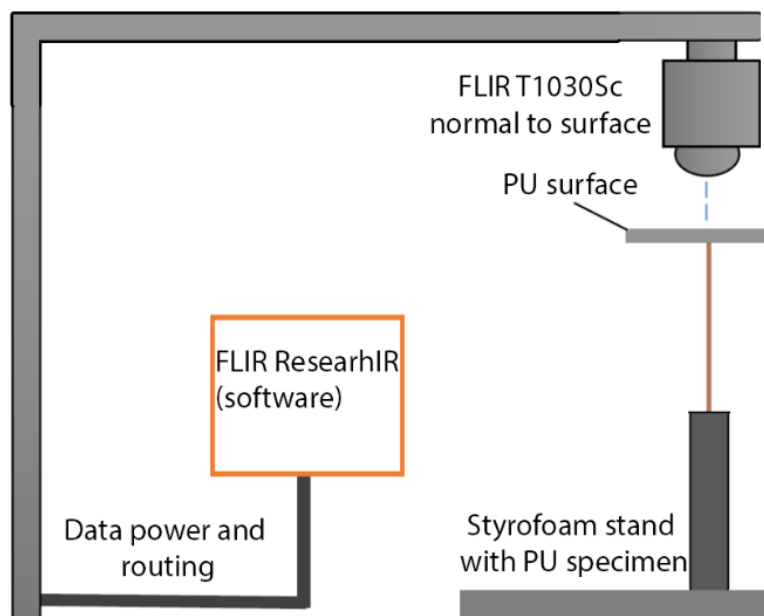

Figure 3: Schematic setup of IR capture

Before the IR images were captured, the samples were brought at a different temperature than the surrounding atmosphere. To obtain the temperature difference for this experiment, the specimens were put in a freezer overnight (approximately 24hrs.). The freezer can hold temperatures of −20°C to −30°C. The surrounding atmosphere (the location of where the IR images were captured) was a steady at 24°C. With a temperature difference between the sample and the atmosphere being established, the IR signatures was captured. IR camera sampling rate was set at $2Hz$. That means, every half second, the software captured the specimen's IR signature. After about 7 minutes, the entire polyurethane specimen had reached 0°C, and the recording was stopped. The red line shown in Figure 4, called the Region of interest, or ROI for short, is the location where the temperature profile for the anti-abrasion specimen was captured. The ROI was at a constant position. This was to ensure that the captured temperature was at the same location on the specimen, throughout the time. For the anti-abrasion sample, nine different temperature profiles were captured, and thirteen different temperature profiles were captured for the anti-seepage. The different captures were because the two different samples reached 0°C at different rates due to size difference and different thermal properties. In preparation for the tests, the specimens were cut into $50 \times 50\ mm$ cubes and labeled A, B and C. The corners of the materials were numbered 1 to 4, and the center was labeled 5. The numbers indicated the point for the measurements of the thickness. This was done for both region of interest for the anti-seepage and the anti-abrasion materials.
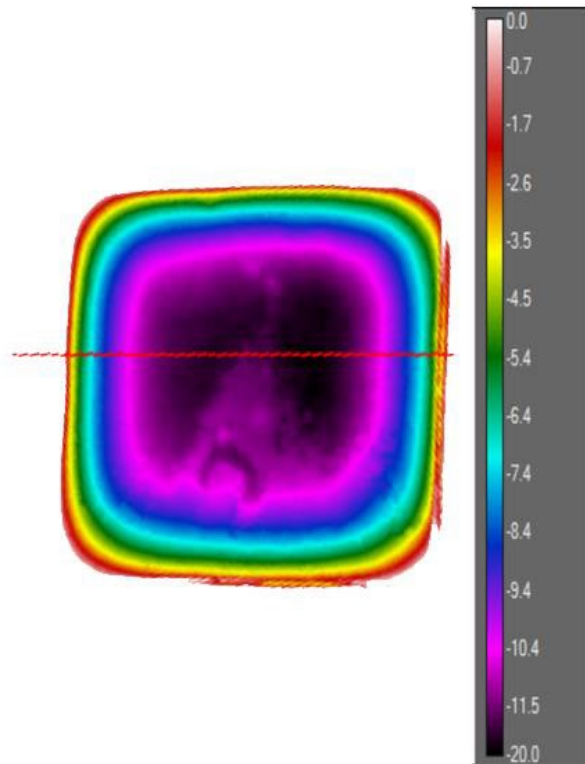

Figure 4: FLIR capture and region of interests where the temperature was read.

The results of these measurements, in millimeters, can be viewed in Table 1 below.

Table 1: Thickness Measurements (mm)

S. No	Anti-abrasion			Anti-seepage		
1	7.15	8.87	10.83	5.25	5.5	5.45
2	8.52	10.35	10.76	5.41	5.65	5.52
3	9.7	8.36	7.9	5.45	6.27	6.4
4	10.025	8.61	8.65	5.38	5.34	6.28
5	10.73	10.73	10.05	5.98	5.45	5.78

When measuring the rate of which heat travels through a material, the thickness of the tested specimen is important. In addition to the length, width and thickness, the masses were measured. The mass for the anti-abrasion material was $16g$ and for anti-seepage was $13g$. Thus, the density of anti-abrasion is $\rho_{anti-abrasion} = 1283 \ kgm^{-3}$ and for anti-seepage: $\rho_{anti-seepage} = 1150 \ kgm^{-3}$.

3. NUMERICAL METHOD TO SOLVE THE HEAT EQUATION

The heat equation is a partial differential equation (PDE), and an analytical solution is difficult to obtain for such an equation [4,25]. Different numerical methods can be applied to solve the problems with the Heat equation and other PDEs [26-29]. One such numerical method is the Finite Difference Method (FDM). When the FDM is applied to a continuous PDE, the numerical solution is replaced with a discrete approximation [30, 31]. This means that the numerical solution is only known at a finite number of positions (boundary and initial conditions). When FDM is applied to a PDE, the first step would be to discretize the physical domain into a finite set of elements or replace the physical domain with a grid, as shown in Figure 5. Here, a two-dimensional plane is divided into a set of finite elements or nodes. The resolution (number of elements) in this example is 11×11. Further, the initial condition here is in the middle, and the boundary conditions are on all edges of the plane. The red square indicates hot areas, and the blue indicates colder areas.
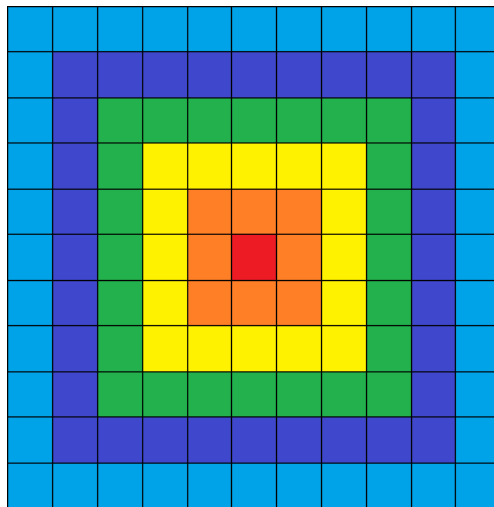

Figure 5: Grid applied to a two-dimensional plane, with the heat source (initial condition) in the middle.

At each of the points, the discrete solution is evaluated. There are two important parameters that govern the accuracy of the results, namely Δx and Δt. Naturally, with smaller Δx and Δt, accuracy increases but the time required to solve the model increases (computationally heavier). Further, the discrete solution to a PDE, (at each node) can be shown to be [30]

$$\frac{\partial \varphi}{\partial x} \approx \frac{\varphi_{i+1} - \varphi_i}{\Delta x} \tag{4}$$

where $\varphi(x, t)$ is the true (continuous) solution, $\varphi(x_i, tm)$ is the continuous solution calculated at each node in the mesh, and φ_i^m is the approximated numerical solution given by solving the FEM equation.

To help the understanding of Equation 4, and the derivation of the approximation of the heat equation, a general grid can be drawn as shown in Figure 6:
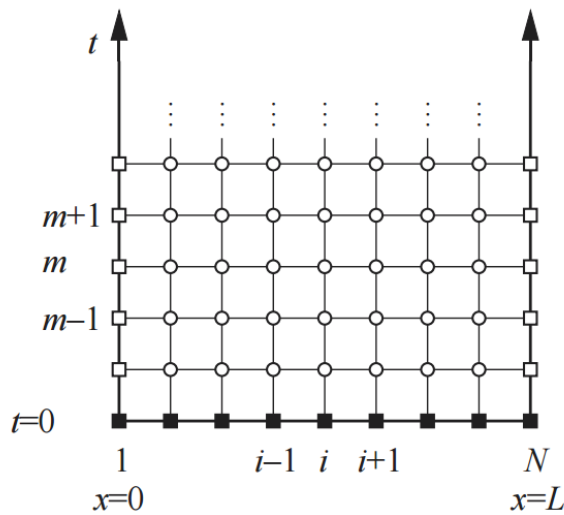

Figure 6: general grid for a one-dimensional Heat equation problem [30]

In Figure 6, the initial condition is displayed as solid squares, and the non-solids squares indicate the boundary conditions. i denote the grid position, m denote the time.

3.1. Forward-Time Central-Space (FTCS) FDM

There are three different types of finite difference approximation: forward, backward and central. The forward difference approximation can be applied to Equation 3, the Heat equation in $x - direction$. By using this technique, the temperature at each node can be estimated one timestep forward, as shown in Equation 5. By further manipulation of the Taylor series, second order PDE can be approximated as shown in Equation 6.

$$\frac{\partial \varphi}{\partial x} \approx \frac{\varphi_i^{m+1} - \varphi_i^m}{\Delta t} \tag{5}$$

$$\frac{\partial^2 \varphi}{\partial x^2} = \frac{\varphi_{i+1} - 2\varphi_i + \varphi_{i-1}}{\Delta x^2} \tag{6}$$

where m denotes the timestep. Equation 5 and 6 can be applied to Equation 3 (Heat equation in $x - direction$) as shown in Equation 7:

$$T_i^{t+1} = T_i^t + \alpha(\frac{T_{i+1}^t - 2T_i^t + T_{i-1}}{\Delta x^2})\Delta t \tag{7}$$

where T is the temperature, i is the space (grid) coordinate of which the temperature is calculated, t is the time, and α is volumetric heat capacity.

Equation 7 is only applicable for a one-dimensional problem. To bring this approximation to a three-dimensional problem, two other space coordinates j and k is introduced. Thus, the final FTCS FEM can be derived [32-34] as given in Equation 8:

$$T_{i,j,k}^{t+1} = T_i^t + \alpha \left(\frac{T_{i+1}^t - 2T_i^t + T_{i-1}}{\Delta x^2}\right)\Delta t + \alpha \left(\frac{T_{j+1}^t - 2T_j^t + T_{j-1}}{\Delta y^2}\right)\Delta t + \alpha \left(\frac{T_{k+1}^t - 2T_k^t + T_{k-1}}{\Delta z^2}\right)\Delta t \tag{8}$$

The advantage of using FTCS is that the values of φ_i^{m+1}, or T_i^{t+1}, can be updated independently of each other [30].

3.2. Numerical Analysis in MATLAB®

The three-dimensional discretized heat equation in cartesian coordinates was initially solved using the FTCS FDM, a numerical method in MATLAB® [35]. Similar studies were done by authors to study numerical analysis in MATLAB® [36,37]. The results were compared with the experiments. As an initial condition, a constant temperature of 249 K was specified throughout the domain. It is vital for the stability and accuracy of the FDM to choose the correct timestep value. The Courant–Friedrichs–Lewy (CFL) condition [38-40] was used to decide the timestep size in this work. The CFL condition is given in Equation (20):

$$2\alpha\Delta t \le min \, ((\Delta x)^2, (\Delta y)^2, (\Delta z)^2) \tag{20}$$

where α is the velocity magnitude, $\Delta t \cong dt$ is the timestep, and $\Delta x = dx$, $\Delta y = dy$ and $\Delta z = dz$ are the distance between mesh elements in three directions.

For solving the heat equation for a total of 6000 timesteps, the following steps were taken: $dt = 1$; seconds; $dx = 0.2$ cm; $dy = 0.2$ cm and $dz = 0.2 \, cm$. The solution can be described in four steps as given in Table 2.

Table 2: Four basic steps to solve the FEM Heat equation

Step	Event	Description
1	Define Parameters	Δt, Δx Δy Δz the spatial domains $spacex$, $spacey$, $spacez$ k and h ρ and c The discretized space Initial temperature and initial conditions
2	Create a matrix, T, containing zeroes	The matrix T, initially only contains zeros. However, in step 3, the temperature at each node will replace the zeroes with the simulated temperature.
3	Create loops	This step is what solves the FTCS FEM. In these loops, both the Δt, Δx are contained. In addition to these, the boundary conditions are included.
4	Plot experimental vs. simulated data	The last step plots the experimental data and compares it with the simulated data from step 1 to 3.

4. RESULTS AND DISCUSSION

Thermal imaging was performed on the polyurethane samples. IR capture software was used to measure the established temperature gradient as a function of time and space. Variation of temperature in anti-abrasion and anti-seepage Polyurethane was recorded by FLIR T1030sc IR thermal camera, as shown in Figures 7 and 8.

Experimental temperature profiles for both Polyurethane were used to obtain values of thermal conductivity (k) and heat transfer coefficient (h) by varying the values of the coefficients in the code until the simulation results closely fit the experimental findings. The results are given in Tables 3 and 4.
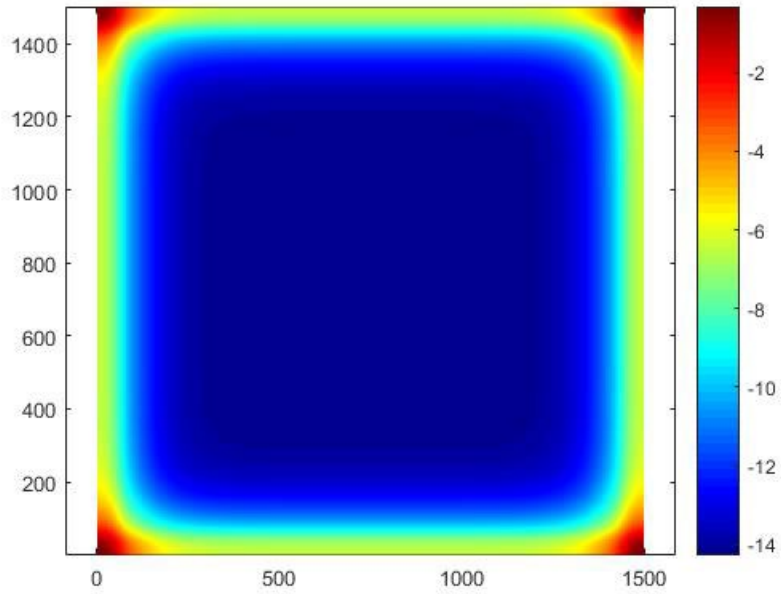
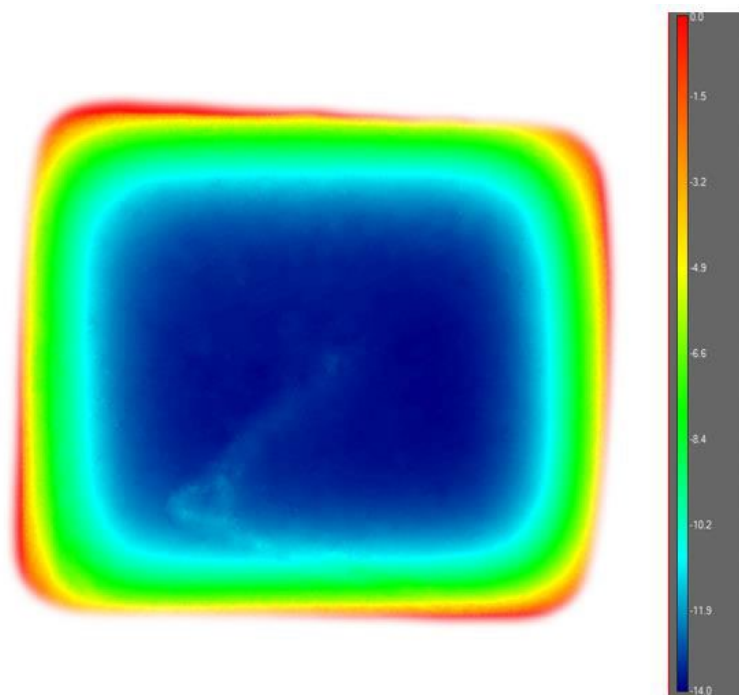Figure 7: the variation of temperature in the anti-seepage Polyurethane after 100 seconds

Figure 8: IR capture (FLIR T1030Sc) of anti-seepage at the same time as the simulation.

Table 3: the coefficient of Heat transfer for anti-abrasion, and anti-seepage Polyurethane

Coefficient of heat transfer (h)	Value ($Wm^{-2}K^{-1}$)
Anti-seepage	19.95
Anti-abrasion	5.2

Table 4: the coefficient of thermal conductivity for anti-abrasion, and anti-seepage Polyurethane

Coefficient of thermal conductivity (k)	Value ($Wm^{-1}K^{-1}$)
Anti-seepage	25.0
Anti-abrasion	11.0

The following graphs show the plotted temperature in the middle of both materials. Figures 9 and 11 show results as a function of time and Figures 10 and 12 as a function of position.

The results reveal that the heat transfer coefficient for anti-abrasion Polyurethane is almost four times that for anti-seepage Polyurethane. The thermal conductivity for the respective has a difference of a factor of two.
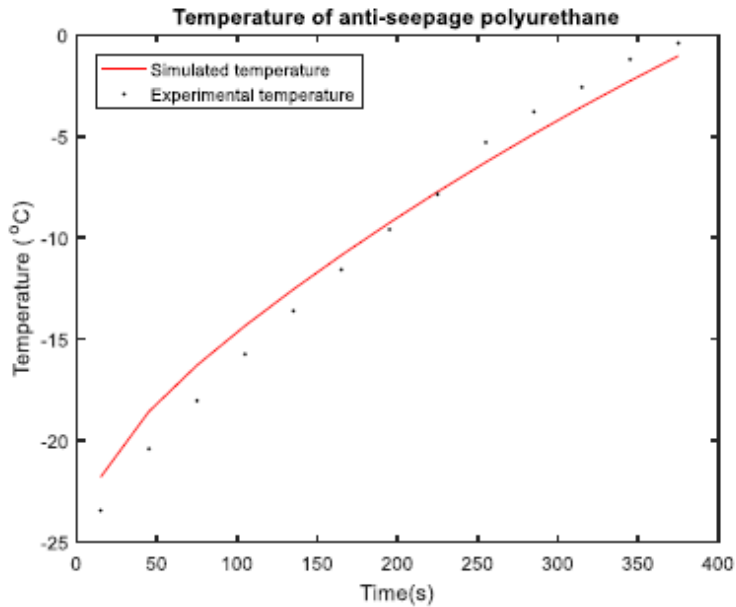

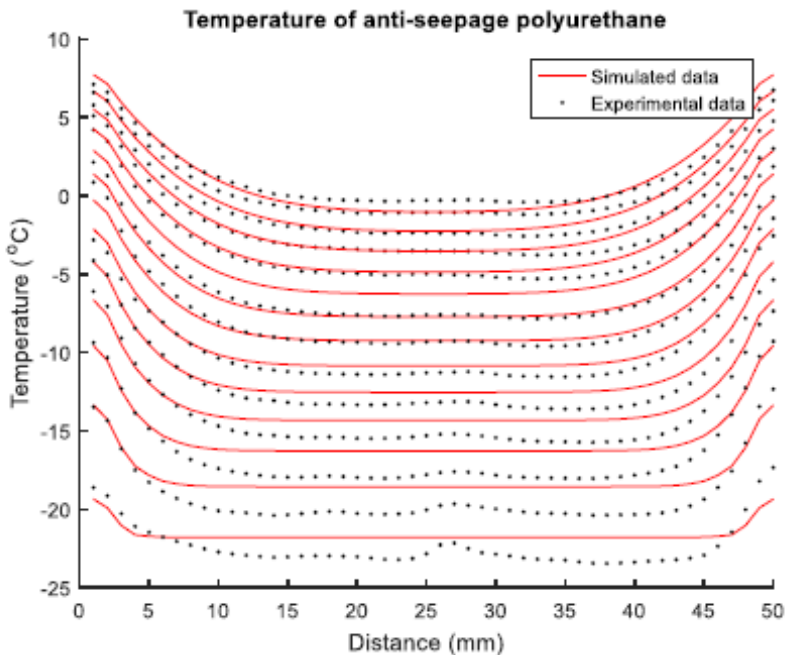Figure 9: Temperature in anti-seepage Polyurethane as a function of time.

Figure 10: Temperature in anti-seepage Polyurethane as a function of position.
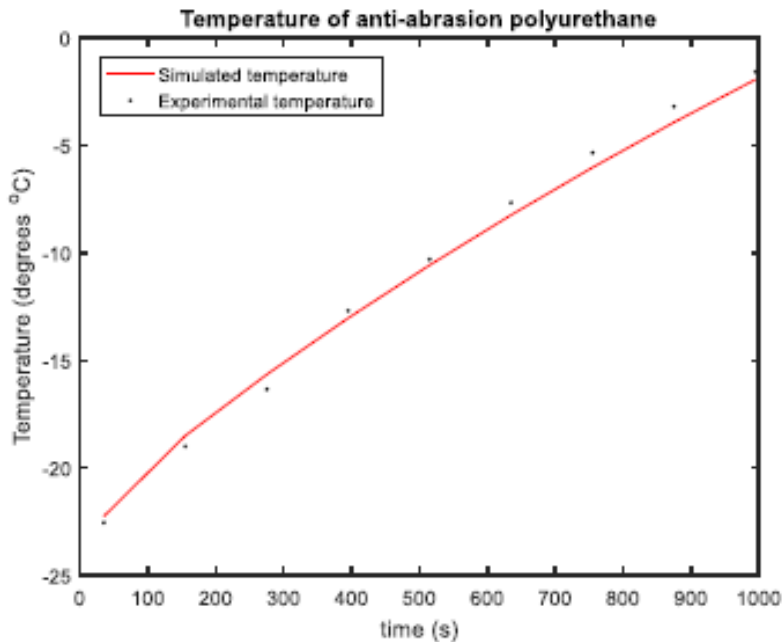

Figure 11: Temperature in anti-abrasion Polyurethane as a function of time.
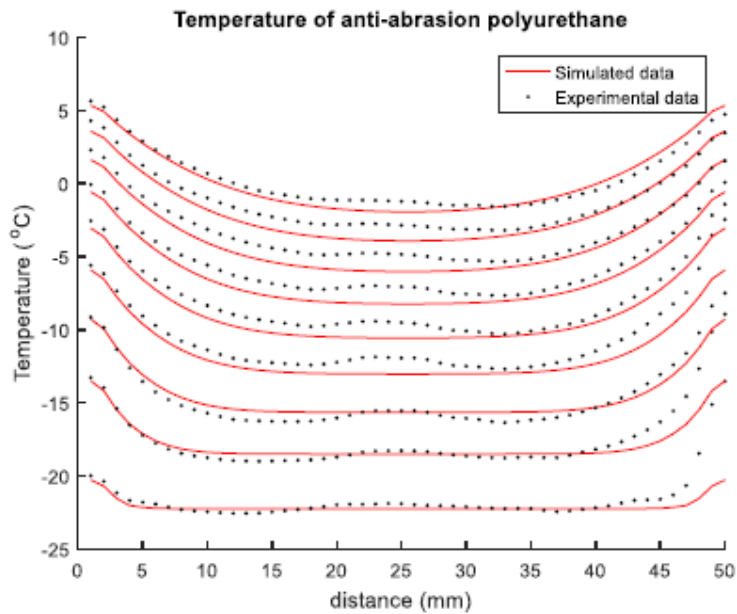
Figure 12: Temperature in anti-abrasion Polyurethane as a function of position.

5. CONCLUSIONS

By applying a finite difference approach to the heat equation, and using IR thermography technology, the two thermal constants, the heat transfer coefficient, and the thermal conductivity coefficient were estimated for anti-abrasion and anti-seepage Polyurethane. The values of the constants reveal that the heat transfer coefficient for anti-abrasion Polyurethane is almost four times that for anti-seepage Polyurethane. The thermal conductivity for the respective has a difference of a factor of two. However, there were a bit variability in the simulated results. This non-uniformity can be due to the presence of air bubbles during the production and curing of Polyurethane samples. Nonetheless, the presented novel method for calculation of thermal properties provides reasonable estimates.

ACKNOWLEDGEMENTS

References

[1] P. Gaspard and T. Gilbert, "Heat conduction and Fourier's law in a class of many particle dispersing billiards," New J. Phys., vol. 10, no. 10, p. 103004, Oct. 2008.

[2] M. J. Moran et al., "Introduction to Thermal Systems Engineering: and Heat Transfer," Engineering, vol. 169, pp. 465–469, 2011, Accessed: May 08, 2022.

[3] T. Rashid, H. Khawaja, and K. Edvardsen, "Determination of Thermal Properties of Fresh Water and Sea Water Ice using Multiphysics Analysis," Int. J. Multiphys., vol. 10, no. 3, pp. 277–290, Sep. 2016.

[4] L. L. Ladislavécsi and Paveí, "Constitutive equation with internal damping for materials under cyclic and dynamic loadings using a fully coupled thermal-structural finite element analysis," Int. J. Multiphys., vol. 3, no. 2, pp. 155–166, Jun. 2009.

[5] Z. Andleeb et al., "Multiphysics Study of Infrared Thermography (IRT) Applications," Int. J. Multiphys., vol. 14, no. 3, pp. 249–271, Sep. 2020.

[6] H. Khawaja, T. Rashid, O. Eiksund, E. Broadal, and K. Edvardsen, "Multiphysics simulation of infrared signature of an ice cube," Int. J. Multiphys., vol. 10, no. 3, pp. 291–302, 2016.

[7] T. Rashid, H. Khawaja, and K. Edvardsen, "Determination of thermal properties of fresh water and sea water ice using multiphysics analysis," Int. J. Multiphys., vol. 10, no. 3, pp. 277–290, 2016.

[8] T. Ahmad, T. Rashid, H. Khawaja, and M. Moatamedi, "Study of the required thermal insulation (IREQ) of clothing using infrared imaging," Int. J. Multiphys., vol. 11, no. 4, pp. 413–426, 2017.

[9] E. Stange, Z. Andleeb, H. Khawaja, and M. Moatamedi, "Multiphysics study of tensile testing using infrared thermography," Int. J. Multiphys., vol. 13, no. 2, pp. 191–202, 2019.

[10] J. Roemer, "The concept of Laser Spot Thermography test rig with real-time data processing," Int. J. Multiphys., vol. 14, no. 1, pp. 31–38, Mar. 2020.

[11] G. Gaussorgues and G. Gaussorgues, "Origins of Infrared Radiation," in Infrared Thermography, Springer Netherlands, 1994, pp. 8–10.

[12] T. Ahmad, T. Rashid, H. Khawaja, and M. Moatamedi, "Study of Wind Chill Factor using Infrared Imaging," Int. J. Multiphys., vol. 10, no. 3, pp. 325–342, Sep. 2016.

[13] H. Khawaja, T. Rashid, O. Eiksund, E. Broadal, and K. Edvardsen, "Multiphysics Simulation of Infrared Signature of an Ice Cube," Int. J. Multiphys., vol. 10, no. 3, pp. 291–302, Sep. 2016.

[14] T. Ahmad, T. Rashid, H. Khawaja, and M. Moatamedi, "Study of the required thermal insulation (IREQ) of clothing using infrared imaging," Int. J. Multiphys., vol. 11, no. 4, pp. 413–426, Dec. 2017.

[15] H.-U. Meier-Westhues, K. Danielmeier, P. Kruppa, and E. Squiller, "Polyurethanes," Jul. 2019.

[16] C. Prisacariu, "Polyurethane Elastomers," 2011.

[17] R. B. Seymour and G. B. Kauffman, "Elastomers: III. Thermoplastic elastomers," J. Chem. Educ., vol. 69, no. 12, pp. 967–970, 1992.

[18] G. Woods and ICI Polyurethanes (Firm), The ICI Polyurethanes book, 2nd ed. Chichester; New York: Published jointly by ICI Polyurethanes and Wiley, 1990.

[19] "China Institute of Water Resources and Hydropower Research (IWHR) - IAHR." https://www.iahr.org/org-center/user?id=12216 (accessed May 08, 2022).

[20] H. Eidesen, Z. Andleeb, H. Khawaja, and M. Moatamedi, "Multiphysics Analysis of Ice-Polyurethane Adhesion under Flexural Loading using FEM Analysis," Int. J. Multiphys., vol. 15, no. 4, pp. 437–452, Dec. 2021.

[21] H. Eidesen, Z. Andleeb, H. Khawaja, and M. Moatamedi, "Multiphysics Analysis of Ice-Polyurethane Adhesion under Flexural Loading using FEM Analysis," Int. J. Multiphys., vol. 15, no. 4, pp. 437–452, Dec. 2021.

[22] L. Qi et al., "Preparation of novel magnetic hydrophobic and lipophilic polyurethane sponge for effective separation of oil/water mixtures," J. Mater. Sci. Mater. Electron. 2021 3222, vol. 32, no. 22, pp. 26291–26305, Oct. 2021.

[23] O. Myrli and H. Khawaja, "Fluid-Structure Interaction (FSI) Modelling of Aquaculture Net Cage," Int. J. Multiphys., vol. 13, no. 1, pp. 97–112, Mar. 2019.

[24] "FLIR T1030sc HD THERMAL IMAGING FOR R&D APPLICATIONS".

[25] K. Chow and A. E. Holdø, "Numerical prediction of indoor temperature stratification," Int. J. Multiphys., vol. 2, no. 4, pp. 355–366, Dec. 2008.

[26] H. A. Khawaja and S. A. Scott, "CFD-DEM Simulation of Propagation of Sound Waves in Fluid Particles Fluidised Medium," Int. J. Multiphys., vol. 5, no. 1, pp. 47–60, Mar. 2011.

[27] D. Brunner, H. Khawaja, M. Moatamedi, and G. Boiger, "CFD modelling of pressure and shear rate in torsionally vibrating structures using ANSYS CFX and COMSOL Multiphysics," Int. J. Multiphys., vol. 12, no. 4, pp. 349–358, Dec. 2018.

[28] H. A. Khawaja, "Review of the phenomenon of fluidization and its numerical modelling techniques," Int. J. Multiphys., vol. 9, no. 4, pp. 397–408, Dec. 2015.

[29] H. Khawaja, "Application of a 2-D approximation technique for solving stress analyses problem in FEM," Int. J. Multiphys., vol. 9, no. 4, pp. 317–324, Dec. 2015.

[30] G. Recktenwald and W. Warni, "Finite-difference approximations to the heat equation Cite this paper Related papers met ode numerik".

[31] E. Hans-Kristian Norum, "Thermal and Mechanical Properties of SK One Component Polyurethane (SKOCP). Determining the Thermal and Mechanical properties of SKOCP in Colder Conditions," 2017. Accessed: May 08, 2022. [Online]. Available: https://munin.uit.no/handle/10037/11352

[32] Z. Andleeb et al., "Thermoelastic Investigation of Carbon-Fiber-Reinforced Composites Using a Drop-Weight Impact Test," Appl. Sci., vol. 11, no. 1, p. 207, Dec. 2020.

[33] A. Leyli, Z. Andleeb, H. Khawaja, R. Messahel, R. Kanna, and M. Moatamedi, "Conjugate Heat Transfer Model Based on SIMPLE and Coupled Energy and Heat Equations," Int. J. Multiphys., vol. 15, no. 1, pp. 29–47, Jan. 2021.

[34] A. Leyli, H. Khawaja, M. Moatamedi, and B. Alzahabi, "Multiphysics Study of Forced Convection Conjugate Heat Transfer (CHT) Problem," Int. J. Multiphys., vol. 13, no. 3, pp. 215–230, Sep. 2019.

[35] "MATLAB - MathWorks - MATLAB & Simulink." https://www.mathworks.com/products/matlab.html (accessed May 09, 2022).

[36] H. Khawaja and M. Moatamedi, "Semi-Implicit Method for Pressure-Linked Equations (SIMPLE) – solution in MATLAB®," Int. J. Multiphys., vol. 12, no. 4, pp. 313–326, Dec. 2018.

[37] A. Nordli and H. Khawaja, "Comparison of Explicit Method of Solution for CFD Euler Problems using MATLAB® and FORTRAN 77," Int. J. Multiphys., vol. 13, no. 2, pp. 203–214, Jun. 2019.

[38] K. Schneider, D. Kolomenskiy, and E. Deriaz, "Is the CFL Condition Sufficient? Some Remarks," Courant–Friedrichs–Lewy Cond., pp. 139–146, 2013.

[39] "The Courant–Friedrichs–Lewy (CFL) Condition," Courant–Friedrichs–Lewy Cond., 2013.

[40] N. Y. Gnedin, V. A. Semenov, and A. V. Kravtsov, "Enforcing the Courant–Friedrichs–Lewy condition in explicitly conservative local time stepping schemes," J. Comput. Phys., vol. 359, pp. 93–105, Apr. 2018.